J. Biomechanics Vol 22, No 4, pp 343-349, 1989
Printed in Great Britain

0021 9290/89 $3.00 + .00


# SURFACE DEFLECTION OF PRIMATE FINGERTIP UNDER LINE LOAD

M. A. SRINIVASAN*

Department of Anesthesiology, Yale University School of Medicine, New Haven, CT 06510, U.S.A.

**Abstract**—A study of the biomechanics of the skin and the subcutaneous soft tissues is of fundamental importance in understanding the process of transduction at the mechanoreceptive nerve terminals responsible for the sense of touch. In the present investigation, the fingertips (distal phalanges) of three adult humans and four monkeys were indented *in vivo* using a line load delivered by a sharp wedge. The resulting skin surface deflection profile was photographed and used as a clue to infer the mechanical nature of the materials that make up the fingertip. It is shown that the modified Boussinesq solution used by Phillips and Johnson (1981), applicable when the fingertip is modeled as an elastic half-space in a state of plane strain, predicts a skin surface deflection profile that can only roughly approximate the empirically observed profiles. As an alternative, a simple model which views the fingertip as an elastic membrane filled with an incompressible fluid (like a 'waterbed') under plane strain conditions is proposed. It is shown that the predictions of this model, which takes into account the finite deformations that occur, agree very well with the photographed profiles in the region of interest (up to about 3 mm from the load).

## INTRODUCTION

Both humans and monkeys primarily use fingertips in the exploration of the external world through the sense of touch. When the fingertips come in contact with an object, the deformation of the skin causes the mechanoreceptive nerve terminals imbedded in the skin to emit electrical impulses whose frequency depends on the type and intensity of deformation. These impulses are then transmitted through the peripheral nerve fibers to the brain where they are appropriately processed and interpreted. The features of the mechanoreceptor response, such as the frequencies of nerve impulses, are directly related to the stresses and strains in the immediate neighborhood of the nerve terminal and, therefore, contain in a coded form, information about the mechanical stimulus. In order to unravel this code, it is important to understand the mechanics of the fingertip.

The fingertip, viewed as a block of material, exhibits complex mechanical behavior—inhomogeneity, anisotropy, rate and time dependence. The gross structure of the fingertip can be described as a flexible membrane (the skin) enclosing soft tissues which are mostly composed of fat. At body temperature, fat is in the form of a liquid, or nearly so (O'Rahilly, 1983). At a finer level, the skin is seen as being composed of two layers, the epidermis and the dermis, which can be further divided into several sublayers. In fact, at the length scale of the mechanoreceptors (5–100 $\mu$m, except for the Pacinian corpuscle, Darian-Smith, 1984), the dermis does not even appear as a material continuum. It consists of five networks: collagen fibers, elastic fibers, blood vessels, nerves and lymphatics (Gibson and Kenedi, 1968). Out of these, the first two are the most important from a mechanical point of view and their complex mechanical behavior has been investigated by Gibson and Kenedi. Additional difficulties arising from irregular inter-connections of the fiber networks make a complete mechanical characterization of the fingertip, viewed as a conglomeration of its constituent fiber networks and tissues, intractable.

Simplification can be achieved by ignoring the details of the structure of the skin and considering it as a membrane. Experimental investigations of its *in vitro* mechanical properties have been performed by many authors (Gibson *et al.*, 1969; Cook *et al.*, 1977; North and Gibson, 1978; Fung, 1981). The mechanical behavior of the skin is so complex that Tong and Fung (1976) found it necessary to define a pseudo strain energy function with thirteen material constants to model the experimental data of Lanir and Fung (1974). For our purpose of understanding the mechanics of the fingertip, of which skin is only one of the constituents, further simplifications are necessary. Even the general theory developed by Danielson (1973, 1977) for an elastic membrane resting on a continuum foundation is too complex for our present needs. Therefore, a reasonable alternative is to develop specialized, simple, tractable models of those aspects of mechanical behavior of the fingertip that are expected to be important.

One such attempt was made by Phillips and Johnson (1981) in their study of mechanoreceptors. They assumed the fingertip to be mechanically equivalent to an incompressible, homogeneous, isotropic, linearly elastic half-space in a state of plane stress or strain. In such a case, for infinitesimal deformations, the Boussinesq solution (Timoshenko and Goodier, 1970) provides the stresses and strains in the medium caused by a line load. Strictly speaking, this solution predicts infinite vertical displacement under the load. Phillips and Johnson used a modified form of the basic

*Received in final form* 17 *December* 1987.

*Current address: Newman Laboratory for Biomechanics and Human Rehabilitation, Department of Mechanical Engineering, MIT, Cambridge, MA 02139, U.S.A.

solution by ignoring its predictions in the immediate vicinity of the load to obtain the strain fields under the various gratings used as stimuli in their recordings of neural response.

Of fundamental importance in their calculations is the skin surface deflection profile under a line load. The present study was motivated by the need to verify experimentally the validity of the Boussinesq solution for *in vivo* fingertip deformation. In essence, the goal of this investigation was to determine whether the primate fingertip as a whole can be modeled as a homogeneous linear elastic solid. The mismatch between the predicted results of the Boussinesq solution and the observed skin surface deflection profile (ref. Fig. 2) prompted the development of an alternative theoretical model.

The model is based on the observation that the structure of the fingertip is essentially like a fluid-filled elastic membrane. In this paper, the equations governing the model behavior are given for the simple case of a line load. Large deformations that usually occur in tactile sensing are taken into account by the model, and it is shown that the model predicts the experimental skin surface deflection profile under line loads much better than the Boussinesq solution. We shall describe the experiments first and then the theoretical model with its predictions.

## METHODS

### *Experimental set up*

A base plate ($45 \times 35 \times 3$ mm) with a triangular prism (which we shall call a 'wedge') on one of its faces was cast using transparent epoxy. The plate was mounted on a tactile stimulator (LaMotte *et al.*, 1983) driven by servo-controlled hydraulic motors. Vertical downward displacement of the plate with the wedge on its underside caused the sharp edge (less than 50 $\mu$m wide and 25 mm long) of the wedge to indent the finger to a desired depth. The vertical displacement and the velocity were both controlled by a minicomputer through pre-programmed local analog feedback circuits. The reactive force of the finger on the wedge was measured with a force transducer in contact with the top of the spring-loaded plate containing the wedge.

An SLR camera with a cable release for the shutter was set up on a micro-manipulator such that the line of collimation was aligned with the length of the wedge. Suitable close-up lenses were mounted onto the camera, resulting in an image that was approximately the same size as the object, the fingertip. A fine grained slow speed film was used.

### *Experimental procedure*

Four anesthetized juvenile *Macaca fascicularis* monkeys, each weighing 4–6 kg and three awake human subjects (25–30 years of age) were used for the experiments. The volar surface of the distal phalanx of the middle finger was chosen as the indentation site with the length of the wedge perpendicular to the length of the finger. Care was taken so that the indentation occurred on the flat part of the distal phalanx, midway between the tip and the joint. The fingernail was glued to a flat, horizontal platform, thereby preventing any translation or rotation of the finger.

The platform with the finger on top was raised till it barely touched the wedge and the force transducer measured a contact force of 1 mN (negligible compared to the forces of indentation which were 0.3–1 N, depending on the depth of indentation). Centering the view finder of the camera on the tip of the wedge, a photograph of the resting state of the fingertip was taken. Subsequently, the finger was indented with a velocity of 1 mm per second until the desired depth of indentation (0.5–2 mm) was reached and the wedge was maintained at that position. During the indentation phase, the force on the finger rose rapidly and started falling during the steady phase. Within about 5 s, it stabilized while the skin surface profile did not change appreciably and a photograph was taken at that time. The wedge was then completely withdrawn and the next trial was begun only after sufficient waiting time to ensure that the finger returned fully to its normal form. Typically, a sequence of increasing indentation depths in steps of 0.25–0.5 mm up to a total of 2 mm were given, while keeping the vertical velocity constant at 1 mm $s^{-1}$ during the indentation phase.

### *Data analysis*

In order to measure the net displacement of the surface of the skin, enlarged images of the photographs were used such that the magnification factor for the fingertip was 20. By superimposing the normal resting profile of the finger with the deformed profile, the net vertical displacements could be measured and plotted.

As mentioned before, our ultimate goal is to apply the results of the present biomechanical investigation to the analysis of mechanoreceptor response. Since the receptor response is dependent on the deformation in its immediate neighborhood which, in turn, is dominated by the loads in the vicinity, higher accuracy is needed in measuring and predicting the skin surface deflection profile in the region close to the line load. Hence, the vertical displacement measurements were taken at horizontal intervals of 0.05 mm up to a distance of 0.5 mm from the wedge tip, and 0.25–0.5 mm steps thereafter.

## RESULTS

The superimposed profiles of the undeformed and the deformed skin surfaces for a monkey and a human fingertip are shown in Fig. 1. Even though all the monkey fingertips were comparable in size to the one

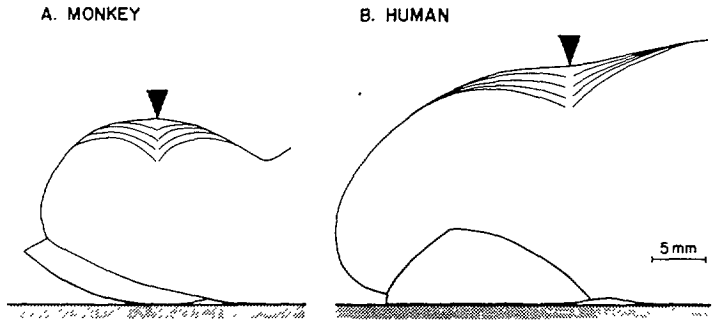


Fig. 1. Superimposed profiles of the undeformed and the deformed skin surfaces for a monkey and a human fingertip drawn to scale. While the rest of the monkey fingers were of the same size as the one shown in (A) their shape was similar to the human finger (B) above and hence approximately flat in the region of deformation. Although the deformed profiles very close to the load (at distances less than 0.05–0.1 mm) could not be observed due to glare, the rest of the profiles were approximately symmetric and circular on either side of the load.

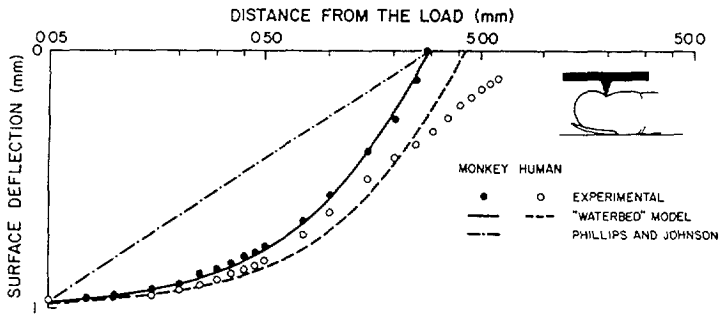


Fig. 2. Experimental and theoretical profiles of the deflection of the skin surface under a line load for both monkey and human. The distance from the load is plotted on a logarithmic scale to emphasize the needed accuracy of model predictions near the load. Experimental data points are the averages of the corresponding points on the left and the right side of the load. It is evident that the Boussinesq solution used by Phillips and Johnson (1981) only roughly approximates the actual profile, whereas the 'waterbed' model proposed here predicts the deflection quite accurately up to about 3 mm from the load.

shown, the pronounced initial surface curvature of the displayed monkey fingertip was absent in the others, and they were similar in shape to the human fingertip shown. For a given depth of wedge indentation, the skin surface deformation was spread over a larger region in the human (6–12 mm from the wedge tip) as compared to the monkey (3–7 mm from the wedge tip). In either case, the deflection profiles were generally symmetrical with respect to the axis of the wedge.

The mean of the surface deflection on either side of the wedge (at 1 mm indentation) is plotted in Fig. 2, so as to eliminate possible small errors occurring due to non-normality of the load to the fingertip surface at the point of contact. In order to emphasize the required accuracy of the predictions of the models very close to the load, a logarithmic scale is chosen for the horizontal distance from the load. It is clear that the modified Boussinesq solution (Phillips and Johnson, 1981) represents the simplest linear approximation to the observed profile of the skin surface deflection when the horizontal distance is expressed in logarithmic units. The 'waterbed' model which, as shown in Fig. 2, is capable of predicting the deflection profile more accurately, is described in detail in the next section.

### *The 'waterbed' model*

We shall now construct a simple, theoretical model of the fingertip which is able to predict the empirically observed deflection profiles in the regions of interest neighboring the location of the load. Once the validity of the model is established, it can then be used to predict the surface profile of the deformed fingertip in more complex loading situations.

As described earlier, the structure of the fingertip can grossly be described as a flexible membrane enclosing soft tissues composed of fat in a liquid state. Also, the thickness of the skin is much less than the overall diameter of the finger. Therefore, we model the fingertip as a membrane of negligible thickness enclosing an incompressible fluid. For further simplification, we ignore the initial curvature of the fingertip and assume it to be in a state of plane strain.

Consider an initially flat, linear-elastic membrane of negligible thickness and width $2L$, resting on an

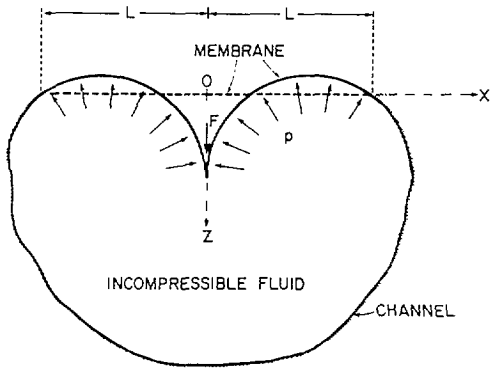


Fig. 3. Schematic showing the physical model on which the mathematical equations are based. The channel wall is considered rigid. The flexible membrane is assumed to have negligible thickness. Its resting state is shown by a horizontal dashed line while its deformed shape under a load $F$ (which is counter-balanced by the fluid pressure $p$) is shown schematically by a continuous line, symmetric about $OZ$.

incompressible fluid enclosed in a rigid-walled channel of arbitrary cross-section, as shown in Fig. 3. The channel with the membrane-covered fluid is assumed to be in a state of plane strain, and the applied load and the membrane stress resultant are expressed as forces per unit length in the direction perpendicular to the cross-section. Let point $O$ on the membrane be chosen as the origin of a Cartesian coordinate system $(X, Z)$ with the positive directions as shown.

Let a downward, concentrated load $F$ be applied at $O$. Since the fluid is incompressible, the deformed shape of the membrane should be such that the area of cross-section of the fluid is preserved (i.e. the area of fluid above the $X$-axis should be equal to the area below), resulting in the deflected shape of the membrane as shown schematically in Fig. 3. Then the particle situated initially at $(X, O)$ on the membrane now occupies a position $(X+U(X), W(X))$ where $U(X)$ and $W(X)$ denote the horizontal and vertical displacements expressed as functions of the initial coordinate $X$. It will be found useful to denote $X+U(X)$ as the final coordinate $x$. Let $w(x)$ denote the vertical displacement as a function of the final coordinate. It is important to recognize that for any arbitrary $X$,

$$W(X)=w(x) \text{ where } x=X+U(X) \tag{1}$$

as is evident from Fig. 4. The distinction between $W(X)$ and $w(x)$ is necessary to clarify what is being measured from the superimposed undeformed and deformed fingertip profiles. We shall now write the governing equations for the deformed configuration, which is symmetric about the load axis.

(i) *Incompressibility constraint.* The incompressibility of the fluid imposes the constraint

$$\int_0^L w(x)\,dx=0 \tag{2}$$

so that the area of cross-section remains the same before and after deformation.

(ii) *Equilibrium of the deformed membrane.*

(a) Under the load at $x=0$ (ref. Fig. 5A)

$$F=2N\sin\theta_0 \tag{3}$$

where $N$ is the membrane force.

(b) For $0<x<L$, equilibrium conditions in the normal and tangential directions to the membrane (ref. Fig. 5B) are

$$N=pR \tag{4}$$

$$N=\text{constant} \tag{5}$$

where $p$ is the fluid pressure, which is constant for a given load $F$, and $R$ is the radius of curvature of the membrane. Because of symmetry of deformation about the load axis, it is sufficient to write and solve the governing equations for $0\leqslant x\leqslant L$. It is well known from differential geometry that

$$R=\frac{\{1+(dw/dx)^2\}^{3/2}}{d^2w/dx^2}. \tag{6}$$

(iii) *Constitutive law for the membrane.* Since the membrane is assumed to be linear elastic,

$$N=E\varepsilon \tag{7}$$

where $E$ is the membrane stiffness, and

$$\varepsilon=\frac{dU}{dX}+\frac{1}{2}\left\{\left(\frac{dU}{dX}\right)^2+\left(\frac{dW}{dX}\right)^2\right\}. \tag{8}$$

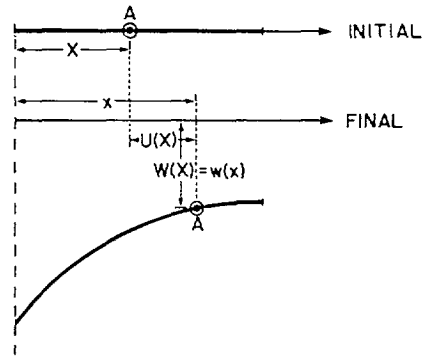


Fig. 4. Initial (before deformation) and final (after deformation) coordinates of a typical material point A on the skin.

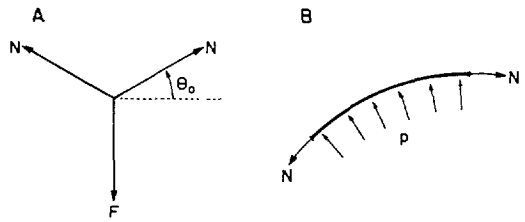


Fig. 5. Free body diagrams at (A) the location of the load $F$ and (B) for an element of the membrane in the deformed state.

Equation (8) is the strain–displacement relation for the Lagrangian (or Green) strain (refer, for example, Fung, 1981).

(iv) *Boundary conditions.* The symmetry condition at $X=0$ and the fixity of the membrane at $X=L$ impose the conditions,

$$U=0 \text{ at } X=0 \text{ and } L \tag{9a}$$

$$W=0 \text{ at } X=L. \tag{9b}$$

*Solution of the equations*

Before we begin to solve the equations, we must express the radius of curvature of the membrane $R$ in terms of the initial coordinate $X$. Since $X=x-U(X)$, we get

$$\frac{dX}{dx}=\frac{1}{(1+dU/dX)}. \tag{10}$$

Therefore, using (1), we obtain

$$\frac{dw}{dx}=\frac{W'}{1+U'} \tag{11a}$$

$$\frac{d^2w}{dx^2}=\frac{W''+W''U'-W'U''}{(1+U')^3} \tag{11b}$$

where number of primes denotes the order of the derivative with respect to $X$. Substitution of (11) in (6) and use of (8) results in

$$R=\frac{(1+2\varepsilon)^{3/2}}{W''(1+U')-W'U''}. \tag{12}$$

We shall now group together all the equations that $U$ and $W$ must satisfy. Since $N$ and $p$ are constants for a given load $F$ in addition to $E$ being a material constant, we see from (4) and (7) that $R$ and $\varepsilon$ must be constants. In addition, the constraint (2) must be satisfied along with the boundary conditions (9).

In order to simplify this set of non-linear differential and integral equations, we assume that $U$ is very small with $U' \ll 1$. We shall also neglect the non-linear term $W'U''$ in the expression for $R$ [equation (12)]. After solving the simplified set of equations, these assumptions will be seen to be justified for the values of $L$ of interest.

To a first approximation, equations (12), (8) and the use of (1) and (10) in (2) give rise to

$$W''=C_1 \tag{13}$$

$$U'+1/2(W')^2=K_1 \tag{14}$$

$$\int_0^L W(X)\,dX=0 \tag{15}$$

respectively. Here $C_1$ and $K_1$ are arbitrary constants.

To solve the set of equations above, we first integrate (13) and satisfy the boundary condition (9b). The $W$ so obtained is then used in (14), the resulting equation is integrated, and the boundary conditions (9a) are satisfied. Thus we obtain for $0 \leqslant X \leqslant L$,

$$W(X)=-\frac{C_1}{2}(L^2-X^2)-C_2(L-X) \tag{16}$$

$$U(X)=\frac{C_1^2X}{6}(L^2-X^2)+\frac{C_1C_2X}{2}(L-X). \tag{17}$$

Use of (16) in (15) results in the relation

$$C_2=-\frac{2}{3}LC_1. \tag{18}$$

Therefore for $0 \leqslant X \leqslant L$, we have

$$W(X)=W_0\left\{3\left(\frac{X}{L}\right)^2-4\left(\frac{X}{L}\right)+1\right\} \tag{19}$$

$$U(X)=\frac{-6W_0^2}{L}\left(\frac{X}{L}\right)\left\{\left(\frac{X}{L}\right)^2-2\left(\frac{X}{L}\right)+1\right\} \tag{20}$$

where $W_0$ denotes the vertical displacement under the load at $X=0$.

*Comparison of theoretical and experimental results*

All the monkey and human fingertips studied (with the possible exception of the monkey fingertip shown in Fig. 1A) could be considered as being approximately flat in their resting state within the region of subsequent deformation. In such a case, with the clarity achieved by the two representations of the vertical displacement $w(x)$ and $W(X)$, we see that the profile obtained experimentally in Fig. 2 is, in fact, $w(x)$. In order to construct the theoretical $w(x)$, we need to shift the location of $W(X)$ by an amount $U(X)$ (as shown in Fig. 4). However, for the values of $L$ and $X$ of interest, if $U(X)$ is sufficiently small, no distinction between $w(x)$ and $W(X)$ need be made. Plotting $W(X)$ as given by (19) with $W_0$ made equal to the experimental value and $L$ chosen so as to have a good least squares fit with the experimental curve, we obtain the theoretical profiles shown in Figs 6 and 7 for each of the monkeys and humans, respectively. Using (19) and (20) it is easily shown that the value of $X$ at which a theoretical curve intersects the abscissa is equal to $L/3$ for that curve and represents the location at which $U(X)$ is maximum. From Figs 6 and 7 we see that the values of $L$ occur between 10 and 15 mm for which the maximum shift due to $U(X)$ (given by $-8W_0^2/9L$) is less than 8% of the $X$-coordinate, and hence negligible. As is evident, the model predicts the profiles very well in the region $X$ less than about 3 mm, much better than the modified Boussinesq solution (ref. Fig. 2).

## DISCUSSION

In modeling the gross mechanical behavior of the fingertip so as to understand the transduction process at the nerve terminals, it is reasonable to neglect the viscoelastic effects for a first analysis. Further simplifying assumptions used by Phillips and Johnson (1981), namely, that the fingertip is mechanically equivalent to an incompressible, homogeneous, isotropic, linearly

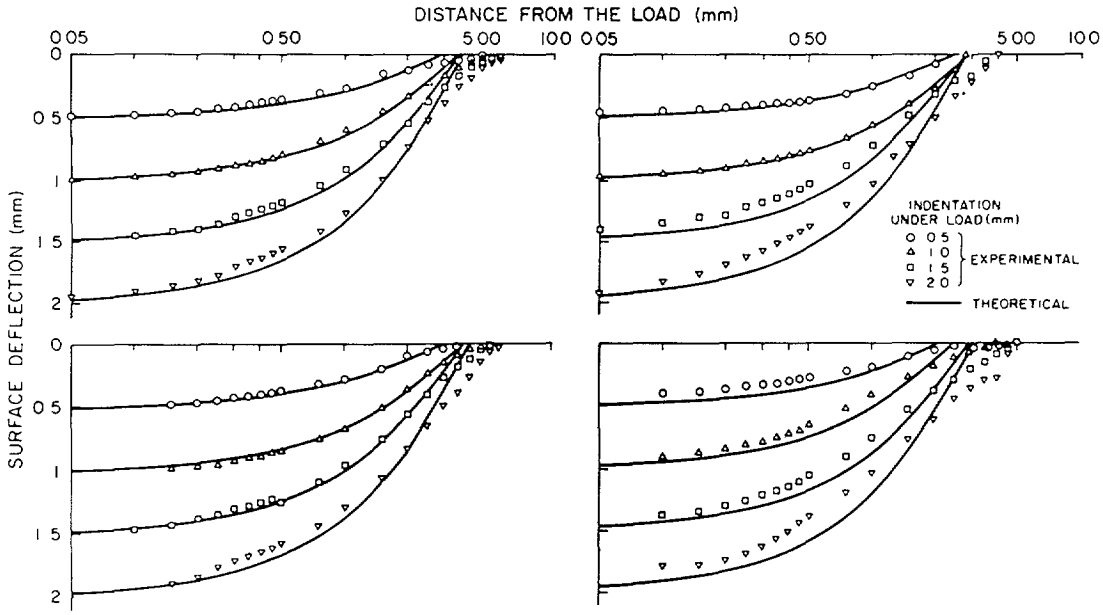


Fig. 6. Experimental skin surface deflection profiles for each of the monkey fingertips and the predictions of the 'waterbed' model for various depths of indentation (0.5, 1, 1.5, and 2 mm under the line load). Experimental data points are the averages of corresponding points on the left and right side of the load.

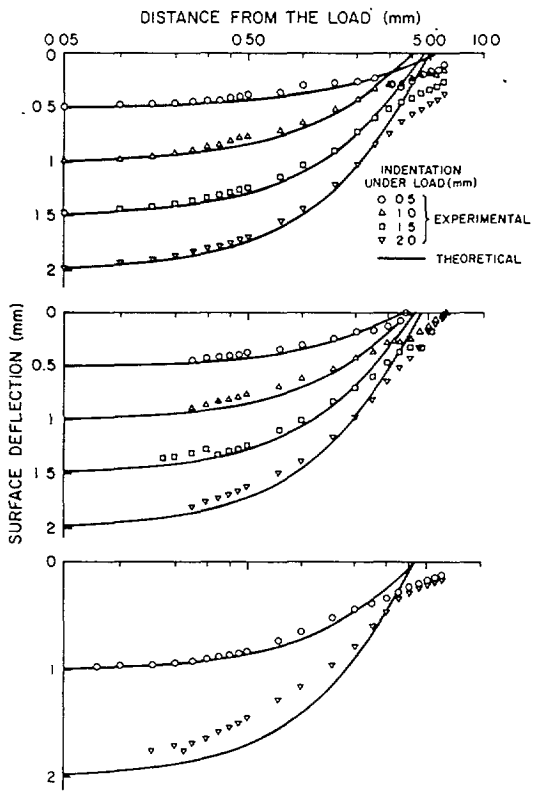


Fig. 7. Experimental skin surface deflection profiles for each of the human fingertips and the predictions of the 'waterbed' model. Same format as in Fig. 6 is followed. Notice that for a given depth of indentation, the region of deformation for a human finger is much higher than that for a monkey finger. For the human subject shown in the bottom panel, only indentations of 1 and 2 mm were given.

elastic half-space in a state of plane stress or strain under infinitesimal deformations, enable the application of the Boussinesq solution to obtain stresses, strains and displacements under a line load. As shown in Fig. 2, the surface deflection profile predicted by the Boussinesq solution only roughly approximates the empirically observed profiles for both monkeys and humans.

Based on the observation that the gross structure of the fingertip is essentially like an elastic membrane filled with an incompressible fluid, the 'waterbed' model has been proposed here. It is demonstrated that this simple model takes into account the large deformations that normally occur in tactile sensing and predicts the skin surface deflection profiles for both monkeys and humans extremely well in the region of interest (up to about 3 mm from the load, Figs 6 and 7). In the region beyond, the model predictions are inaccurate. Indeed, the bulging (i.e. $W<0$) predicted by the model in the region $L/3<X<L$ is not observed in the experimental profile. This bulging is a consequence of the assumptions of plane strain and incompressibility. In the actual finger, while incompressibility is expected to be satisfied quite well, the extra volume of fluid due to the indentation flows in the direction of the length of the wedge and increases the width of the finger and the length of contact. However, as observed by Phillips and Johnson (1981), responses of slowly and quickly adapting mechanoreceptors are not influenced by typical loads at distances of more than about 3 mm. Hence, the errors in the predicted deflection profile beyond 3 mm from the line load are not serious for our purpose, and the negative values of $W$ at the bulge should be neglected

as an artifact of the model. These errors could be eliminated by a three-dimensional version of the model.

In order to see an interesting implication of the model, consider equations (4) and (5). When plane strain conditions are satisfied under any object whose cross-sectional shape is arbitrary, wherever the membrane surface is not in contact with the object, these equations are valid. Since for a given object applied at a specified load the fluid pressure, $p$, is constant, we have the result that the radius of curvature $R$ should be constant. Thus, either the membrane surface conforms to the shape of the object wherever it is in contact or has a circular profile wherever it is not. The *free* skin surface therefore assumes a circular cylindrical shape under plane strain loading conditions (as is evident in the empirically observed profiles shown in Fig. 1). This particular implication has been noted earlier by Taylor and Lederman (1975). Indeed, it can be demonstrated similarly that in the general three-dimensional case when plane strain assumptions do not hold, the free skin surface should assume a spherical shape wherever it is not in contact with the indenting object, while conforming to the surface of the object elsewhere. However, for further accuracy in modeling the mechanical behavior of the fingertip, it may be necessary to take into account the finite thickness and the bending rigidity of the skin, especially in regions where bending is severe. This is supported by the fact that the accuracy of the predictions of the current model reduces as the depths of indentation increase. Furthermore, under higher depths of indentation, the observed deflections within 3 mm the load for all the cases shown in Figs 6 and 7 are always lesser than the model predictions, indicating that the actual fingertip is stiffer than the waterbed model that neglects the membrane thickness.

*Acknowledgements*—The author wishes to thank Professor Robert H. LaMotte for the discussions, constant support and encouragement. He is also indebted to James Whitehouse for all of his help, David Reddy for the computer programs, and Laurie Hauer for typing this manuscript. This work was supported by NIH Grant NS 15888.

## REFERENCES

Cook, T., Alexander, H. and Cohen, M. (1977) Experimental method for determining the two-dimensional mechanical properties of living human skin. *Med. biol. Engng Comput.* **15,** 381–390.

Danielson, D. A. (1973) Human skin as an elastic membrane. *J. Biomechanics* **6,** 539–546.

Danielson, D. A. (1977) Wrinkling of the human skin. *J. Biomechanics* **10,** 201–204.

Darian-Smith, I. (1984) The sense of touch: performance and peripheral neural processes. *Handbook of Physiology—The Nervous System.*, Vol. III, pp. 739–788. Am. Physiol. Soc. Bethesda, MD.

Fung, Y. C. (1981) *Biomechanics.* Springer, New York.

Gibson, T. and Kenedi, R. M. (1968) The structural components of the dermis and their mechanical characteristics. *The Dermis, Advances in Biology of Skin* (Edited by Montagna, W., Bentley, J. P. and Dobson, R. L.). *Proc. Symp. Biology of Skin* **10,** 19–38.

Gibson, T., Stark, H. and Evans, J. M. (1969) Directional variation in extensibility of human skin *in vitro*. *J. Biomechanics* **2,** 201–204.

LaMotte, R. H., Whitehouse, G. M., Robinson, C. J. and Davis, F. (1983) A tactile stimulator for controlled movements of textured surfaces across the skin. *J. electrophysiol. Tech.* **10,** 1–17.

Lanir, Y. and Fung, Y. C. (1974) Two-dimensional mechanical properties of rabbit skin: I—experimental system; II—experimental results. *J. Biomechanics* **7,** 29–34, 171–182.

North, J. F. and Gibson, F. (1978) Volume compressibility of human abdominal skin. *J. Biomechanics* **11,** 203–207.

O'Rahilly, R. (1983) *Basic Human Anatomy*, pp. 27–32. W. B. Saunders, Philadelphia.

Phillips, J. R. and Johnson, K. O. (1981) Tactile spatial resolution. III. A continuum mechanics model of skin predicting mechanoreceptor response to bars, edges and gratings. *J. Neurophysiol.* **46,** 1204–1225.

Taylor, M. M. and Lederman, S. J. (1975) Tactile roughness of grooved surfaces: a model and the effect of friction. *Perception Psychophys.* **17,** 23–36.

Timoshenko, S. and Goodier, J. N. (1970) *Theory of Elasticity.* McGraw-Hill, New York.

Tong, P. and Fung, Y. C. (1976) The stress–strain relationship for the skin. *J. Biomechanics* **9,** 649–657.